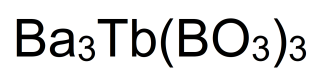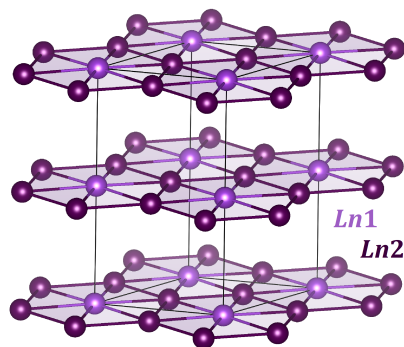Graphical Abstract

Structure and magnetism of a new hexagonal polymorph of $Ba_3Tb(BO_3)_3$ with a quasi-2D triangular lattice

Nicola D. Kelly, Cheng Liu, Siân E. Dutton

$Ba_3Tb(BO_3)_3$

$P6_3cm$

Highlights

Structure and magnetism of a new hexagonal polymorph of $Ba_3Tb(BO_3)_3$ with a quasi-2D triangular lattice

Nicola D. Kelly, Cheng Liu, Siân E. Dutton

- New low-temperature polymorph of $Ba_3Tb(BO_3)_3$ has been synthesised

- Quasi-2D triangular lattice of magnetic ions shows no long range order down to 2 K

- Possible short-range ordering below 10 K

- Inverse magnetocaloric effect below 4 K

Structure and magnetism of a new hexagonal polymorph of $Ba_3Tb(BO_3)_3$ with a quasi-2D triangular lattice

Nicola D. Kelly, Cheng Liu, Siân E. Dutton[*]

Abstract

This article reports the structural and magnetic characterisation of a new hexagonal ($P6_3cm$) low-temperature phase of $Ba_3Tb(BO_3)_3$, isostructural with the heavier lanthanide borates with formula $Ba_3Ln(BO_3)_3$ (Ln = Dy–Lu). The crystal structure contains a quasi-two-dimensional (2D) triangular lattice of Tb^{3+} ions and is predicted to display unusual magnetic behaviour as a result of the low dimensionality. Magnetic susceptibility $\chi(T)$ shows antiferromagnetic interactions ($\theta_{CW} = -7.15$ K) and no sharp ordering transition at $T \geq 2$ K, but analysis of $\chi'(T)$, isothermal magnetisation and heat capacity suggests the possibility of short-range ordering at $T \approx 10$ K. The material exhibits an inverse magnetocaloric effect at $T < 4$ K.

Keywords: lanthanide, borate, magnetism, triangular lattice, two-dimensional

1. Introduction

A unique ordered ground state is possible on a square plaquette of magnetic spins with antiferromagnetic nearest-neighbour interactions, but not on a triangular plaquette (Fig. 1). This idea of geometric 'frustration' can be extended to cover lattices in two or three dimensions (2D/3D) with a large number of spins, including more complex arrangements such as the kagome, garnet and pyrochlore lattices [1, 2]. From this simple observation comes a vast body of theoretical and experimental work on the manifestation of these lattices in real materials.

---

[*]Corresponding author
   Email address: sed33@cam.ac.uk (Siân E. Dutton)

Frustration leads to degeneracy of the ground state and lowering or complete suppression of the magnetic ordering transition temperature. Some geometrically frustrated magnets (GFMs) have been proposed as quantum spin liquids (QSLs): states where the spins are highly entangled over long distances, but which do not exhibit either magnetic ordering or spin-freezing down to the lowest measured (millikelvin) temperatures [3, 4]. The quasi-2D triangular QSL candidate $YbMgGaO_4$ is a well-known example [4–7]. There is no magnetic site mixing, producing a structurally perfect quasi-2D triangular lattice which does not order down to 60 mK [5]. There is, however, random site disorder between Mg^{2+} and Ga^{3+} in the non-magnetic layers, which is expected to affect the crystal electric field environment of the Yb^{3+} ions by distorting the local Yb–O geometry. A number of experimental studies have postulated that this factor is crucial in producing the QSL phase [8, 9], while others predict that it should lead to spin-glass behaviour rather than a QSL [6, 10, 11]. Further examples include $PrMgAl_{11}O_{19}$, $NdMgAl_{11}O_{19}$, $KBaLn(BO_3)_2$ and $RbBaLn(BO_3)_2$, which feature perfect triangular lattices of magnetic ions but again suffer from non-magnetic site disorder [12–15], and the completely disorder-free $NaYbO_2$ which is a promising QSL candidate [16, 17]. In other materials the triangular lattice is distorted from perfect equilateral geometry, which may lead to commensurate or incommensurate magnetic ordering as the lattice is less frustrated [18–22].
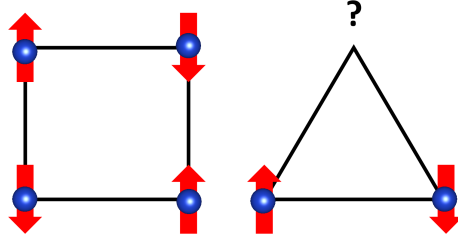

Figure 1: Geometric frustration of magnetic spins on square and triangular plaquettes.

Layered borates with the general formula $Ba_3Ln(BO_3)_3$ were first reported in 1993 by Ilyukhin and Dzhurinsky for $Ln =$ Dy, Ho, Tm, Yb, Lu, with two different structures: a trigonal unit cell for $Ba_3Dy(BO_3)_3$ and a hexagonal unit cell for the samples with $Ln =$ Ho–Lu [23]. These two crystal structures are shown in Fig. 2, highlighting the

arrangement of the lanthanide ions in each case. Both polymorphs of $Ba_3Ln(BO_3)_3$ contain triangular BO_3^{3-} groups and 9-coordinate Ba^{2+} ions. In the trigonal polymorph the lanthanide ions are arranged in closely spaced chains parallel to the c-axis, with adjacent chains slightly offset along that direction, while in the hexagonal polymorph the lanthanide ions form an eclipsed, quasi-2D triangular lattice parallel to the ab plane. The compounds $Sr_3Ln(BO_3)_3$ also crystallise in the trigonal structure type [24]. A later study [25] found $Ba_3Dy(BO_3)_3$ to have the hexagonal crystal structure, and in 2018, magnetic susceptibility measurements of the isostructural series $Ba_3Ln(BO_3)_3$ (Ln = Dy–Yb) were reported [26]. This revealed antiferromagnetic nearest-neighbour interactions with neither long-range order nor glassiness at $T \geq 2$ K, indicating that the compounds are geometrically frustrated and could be considered QSL candidates. A further study on $Ba_3Yb(BO_3)_3$ used nuclear magnetic resonance (NMR) spectroscopy to show an absence of spin ordering or freezing down to $T = 0.26$ K, including in high fields up to 15.8 T [27].

This article reports the synthesis, structural analysis and magnetic characterisation of a new hexagonal polymorph of $Ba_3Tb(BO_3)_3$, shown to be isostructural with the $Ba_3Ln(BO_3)_3$ analogues where Ln = Dy–Lu. Like the latter compounds, the new phase reported here displays no sharp magnetic ordering transition above 2 K, consistent with low-dimensional behaviour.

2. Experimental

A polycrystalline sample of hexagonal $Ba_3Tb(BO_3)_3$ was synthesised according to a ceramic procedure, adapted from ref. 26, from $BaCO_3$ (Alfa Aesar, 99.997 %), H_3BO_3 (Alfa Aesar, 99.999 %) and Tb_4O_7 (Alfa Aesar, 99.998 %). Stoichiometric amounts of the reagents were ground with a pestle and mortar and placed in an alumina crucible. The powder was first heated in air at 500 °C for 12 h in order to decompose $BaCO_3$ and H_3BO_3. The sample was subsequently cooled, reground, pressed into a 13 mm pellet and reheated in air to 875 °C for several days with regrinding every 12 hours. Samples of $Ba_3Ln(BO_3)_3$ (Ln = Gd, Dy, Ho, Er, Y) were prepared in the same way from the relevant rare earth oxides and heated for 24 h at 900 °C. Each sample was
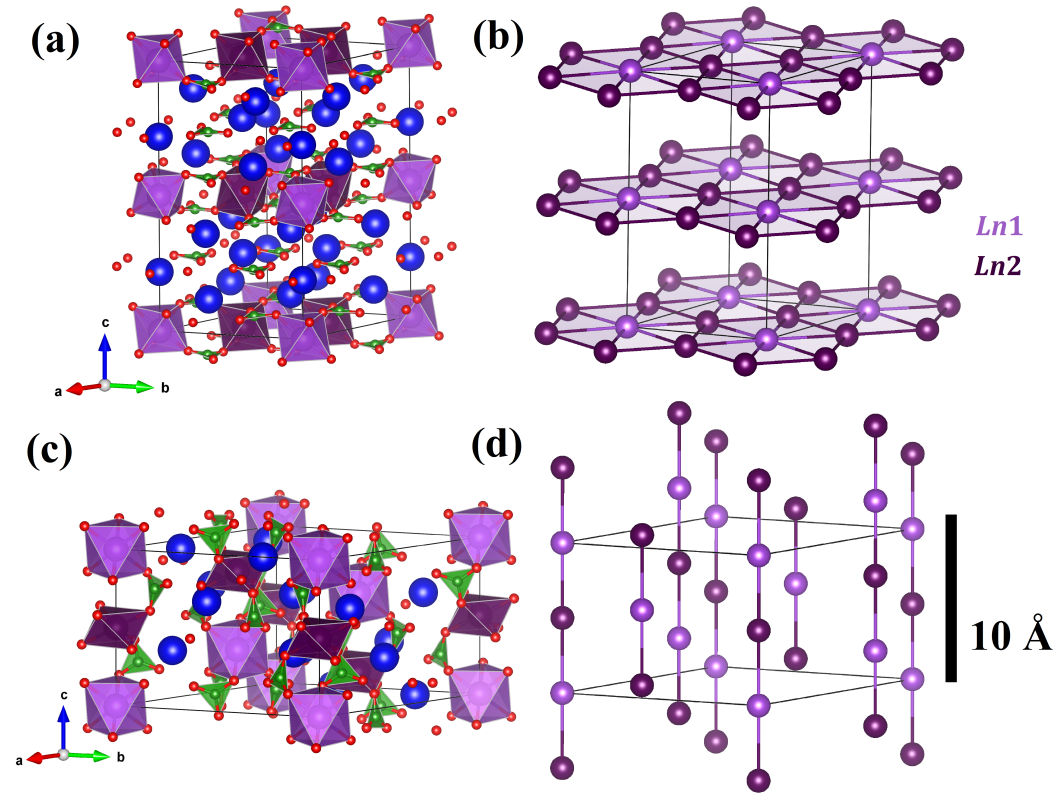
Figure 2: Polyhedral models and magnetic lattices of the hexagonal $P6_3cm$ (a,b) and trigonal $R\bar{3}$ (c,d) polymorphs of $Ba_3Ln(BO_3)_3$. Ln atoms and polyhedra in purple, Ba atoms in blue, B atoms in green and O atoms in red. All structures are shown on the same scale.

then repelletised and reheated several times with the reaction temperature increasing in 50 °C increments up to 1250 °C.

Room temperature powder X-ray diffraction (PXRD) patterns were collected on a Bruker D8 diffractometer (Cu Kα, λ = 1.541 Å) in the range $10 \leq 2\theta(°) \leq 90$ with a step size of 0.01°, 1 second per step. Low-temperature measurements, $12 \leq T(\text{K}) \leq 300$, were taken on cooling with the same diffractometer using an Oxford Cryosystems PheniX stage. The sample stage was allowed to thermalise at each temperature for 20 minutes before measuring across the range $10 \leq 2\theta(°) \leq 70$, step size 0.02°, 0.6 seconds per step. Rietveld refinement [28] was carried out using the program TOPAS [29].

Magnetic susceptibility was measured on a Quantum Design MPMS 3 in the temperature range $2 \leq T(\text{K}) \leq 300$. Isothermal magnetisation was measured on a Quantum Design PPMS Dynacool using the ACMS-II option in the field range $0 \leq \mu_0 H(\text{T}) \leq 14$. In a low field of 500 Oe, the $M(H)$ curve is linear for all T and the susceptibility can therefore be approximated by $\chi(T) = M/H$. Zero-field heat capacity was measured on the PPMS in the temperature range $2 \leq T(\text{K}) \leq 30$. Samples were mixed with an equal mass of Ag powder (Alfa Aesar, 99.99 %, –635 mesh) to improve thermal conductivity before being pressed into a 1 mm thick pellet for measurement. Apiezon N grease was used to provide thermal contact between the sample platform and the pellet. The contribution of Ag to the total heat capacity was subtracted using values from the literature [30] and the $Ba_3Tb(BO_3)_3$ lattice contribution was estimated and subtracted using a Debye model with θ_D = 255 K [31].

3. Results and Discussion

3.1. Crystal Structure

The structure of the new phase was investigated using PXRD (Fig. 3; Table 1) and found to be isostructural with the heavier $Ba_3Ln(BO_3)_3$ analogues, Ln = Dy–Lu (space group $P6_3cm$); no reflections from the high-temperature $R\bar{3}$ phase were observed. The heavier Ba and Tb atoms scatter X-rays much more strongly than B or O. In the refinement, therefore, the B and O atoms were fixed at the positions taken from the

5

isostructural compound, $Ba_3Yb(BO_3)_3$ [25].

The presence, if any, of Ba^{2+}/Tb^{3+} site disorder was tested by setting a suitable mixed cation occupancy in each of the six metal sites and refining partial occupancies with the overall stoichiometry fixed at 3:1. No significant site disorder was observed, in agreement with previous results for this structure type [23, 25, 26, 32]. The result is as expected given the large difference in ionic radii between Ba^{2+} (135 pm) and Tb^{3+} (92.3 pm; each radius given for a 6-coordinate ion) [33]. The nearest-neighbour Tb–Tb distances (within the layers) are 5.45232(8) Å (Tb1–Tb2) and $\frac{a}{\sqrt{3}}$ = 5.45193(4) Å (Tb2–Tb2), while the perpendicular interlayer distance is $\frac{c}{2}$ = 8.86021(8) Å. The 2D layers are thus distorted from perfectly equilateral triangles, but the deviation in bond angle is smaller than 0.01 %. This value is small compared with other 2D triangular lattice compounds such as the lanthanide orthoborates LnBO$_3$ (1.5 % deviation) and RbBaLn(BO$_3$)$_2$ (2.5 % deviation) [15, 34].
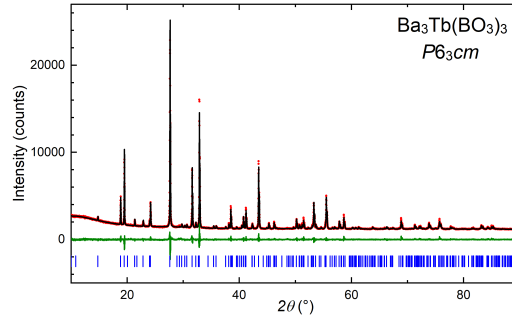

Figure 3: Room temperature PXRD pattern for $Ba_3Tb(BO_3)_3$ ($P6_3cm$): Red dots – experimental data; black line – calculated intensities; green line – difference pattern; blue tick marks – Bragg reflection positions.

Crystallographic studies in the 1990s, including both powder and single-crystal studies, found that $Ba_3Ln(BO_3)_3$ crystallises in the hexagonal space group $P6_3cm$ for the smaller ions, Ln = Dy, Ho, Y, Er, Tm, Yb, Lu and Sc, but the trigonal space group $R\bar{3}$ for the larger Ln = Pr–Tb [25, 32]. Analysis of the solid solution $Ba_3Y_{1-x}Eu_x(BO_3)_3$ gave a limit of x = 0.20(5) for incorporation of the larger Eu^{3+} ion into the hexagonal structure. This limit corresponds to a maximum effective Ln^{3+} radius of 1.049(2) Å, consistent with the 6-coordinate Dy^{3+} crystal radius of 1.052 Å [33]. Our study finds

Table 1: Atomic positions for $Ba_3Tb(BO_3)_3$ ($P6_3cm$). The refined lattice parameters are: $a = b = 9.44302(6)$ Å; $c = 17.72041(15)$ Å; $V = 1368.440(20)$ Å^3 (Z = 6). The goodness-of-fit parameter $\chi^2 = 3.11$ and $R_{wp} = 7.47$. B and O atomic positions are taken from reports of the isostructural $Ba_3Yb(BO_3)_3$ [25] and were not refined. B_{iso} was fixed at 1 Å^2 for all atoms.

Atom	Site	x	y	z
Tb1	2a	0	0	0
Tb2	4b	2/3	1/3	0.9963(3)
Ba1	2a	0	0	0.2262(5)
Ba2	4b	2/3	1/3	0.2711(4)
Ba3	6c	0.3409(13)	0.3409(13)	0.1307(6)
Ba4	6c	0.3227(13)	0.3227(13)	0.3682(5)
B1	6c	0.341	0.341	0.575
B2	6c	0.345	0.345	0.746
B3	6c	0.332	0.332	0.922
O1	6c	0.187	0.187	0.584
O2	12d	0.328	0.478	0.574
O3	12d	0.185	0.336	0.746
O4	6c	0.483	0.483	0.747
O5	12d	0.338	0.476	0.921
O6	6c	0.196	0.196	0.932

that the maximum Ln^{3+} radius is greater than previously reported, at 1.063 Å, the crystal radius of Tb^{3+}.

For certain compounds, particularly $Ba_3Dy(BO_3)_3$, there is debate in the literature over the melting point and whether or not the hexagonal phase transforms into the trigonal phase at high temperatures [25, 32, 35]. Fig. 4 summarises the structural parameters for all $Ba_3Ln(BO_3)_3$ phases reported so far. The existence of both $R\bar{3}$ and $P6_3cm$ polymorphs for $Ln = $ Dy, Tb, depending on the synthesis conditions, raised the possibility of other polymorphs of $Ba_3Ln(BO_3)_3$ being achievable. We observed full conversion from the hexagonal to the trigonal structure for $Ln = $ Dy, Ho and Er (but not Yb or Lu) when heated at higher temperatures in the range 1050–1250 °C, as found by Simura *et al.* [35]. It is plausible that synthesis at lower temperatures might produce hexagonal $Ba_3Gd(BO_3)_3$, but this is unlikely to be the case for even lighter Ln, as a larger Ln:A radius ratio ($A = $ Ba, Sr) favours the trigonal structure: the compounds with $A = $ Sr exhibit only the trigonal phase [24].
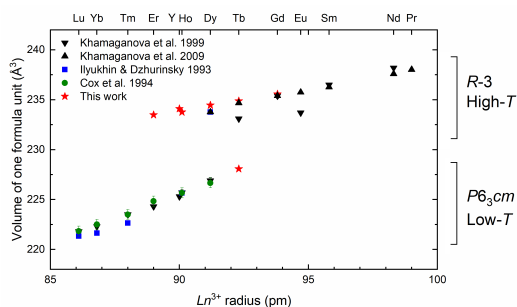

Figure 4: Unit cell volumes of $Ba_3Ln(BO_3)_3$ compounds as a function of lanthanide ionic radius [23, 25, 32, 36].

The low-temperature phase of $Ba_3Tb(BO_3)_3$ is stable when heated from room temperature up to the synthesis temperature (875 °C) for prolonged periods of time, e.g. 1 week or more. Heating at $T \geq 900$ °C gradually converts it to the trigonal structure. At this temperature the conversion took about 360 hours, i.e. 15 x 24 hours with intermediate regrinding (see Supplementary Information, Fig. S1), but the process is faster at higher temperatures. The process is reversible: prolonged heating at $T \leq 875$ °C produces the hexagonal phase once more.

Variable-temperature PXRD was carried out on the new low-temperature phase of $Ba_3Tb(BO_3)_3$. No structural phase transition was observed on cooling from 300 to 12 K. The refined lattice parameters are given in Fig. 5. The a lattice parameter shows a monotonic decrease on cooling but the c parameter (interplanar spacing) first decreases on cooling to 100 K, followed by a steady increase on further cooling. No low-temperature measurements on other $Ba_3Ln(BO_3)_3$ polymorphs have been reported, but similar behaviour has been observed in the layered compound α-$SrCr_2O_4$ and in Ruddlesden-Popper oxides; in both cases this is associated with distortions of the layers [20, 37]. Rietveld refinements at each temperature showed no significant changes in the Tb atomic positions across the range 12–300 K, indicating that the magnetic layers retain their 2D triangular geometry, but there was a steady decrease in the z-position of the Ba1 site by 4 % on cooling from 300 K to 12 K (see Supplementary Information, Fig. S2). The changes in lattice parameters may also be related to changes in the B and O atomic positions, which cannot be observed directly using XRD; variable-temperature neutron diffraction studies are required to investigate this further. It is also plausible that this structural behaviour may be related to competition between polymorphs which coexist at a local level in the same sample [38, 39]; in this case diffuse scattering measurements would be the key to solving the problem.

3.2. Bulk magnetic properties

The DC magnetisation was measured on warming from 2 to 300 K in a field of 500 Oe after cooling the sample from 300 K in zero magnetic field (ZFC) (Fig. 6) using a Quantum Design MPMS 3. Linear Curie-Weiss fitting, $\chi = C/(T - \theta_{CW})$, was carried out in both high-temperature (150–300 K) and low-temperature (20–50 K) regimes, in order to account for thermal population of excited states at higher temperatures [15]. The resulting magnetic parameters are given in Table 2. The effective magnetic moment per Tb^{3+} ion was calculated from the Curie constant using $\mu_{eff}(\mu_B) = \sqrt{8C}$ for both fitting regimes and agrees with the theoretical free-ion value $g_J\sqrt{J(J+1)}$ within experimental error. The Curie-Weiss temperature θ_{CW} is negative, indicating antiferromagnetic interactions. Geometric frustration was quantified using the frustration parameter $f = |\theta_{CW}/T_0|$, where $f > 10$ usually indicates strong frustration [1], and the
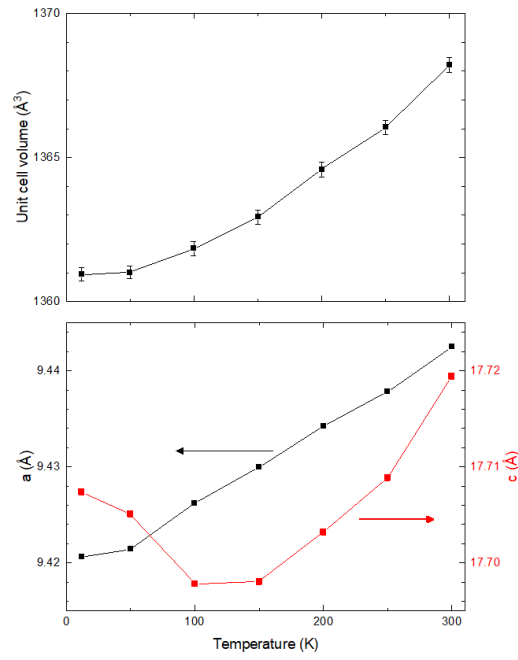
Figure 5: Lattice parameters of $Ba_3Tb(BO_3)_3$ ($P6_3cm$), from PXRD, as a function of temperature. For a and c some error bars are smaller than the datapoints. Solid lines are a guide to the eye.

resultant ranges are given in Table 2. Further experiments are required in order to find T_0 and accurately assess the frustration of the magnetic lattice. Crystal field effects as well as short- and long-range dipolar interactions between the $^7F_6$ Tb^{3+} ions are expected to contribute to the measured Curie-Weiss temperature [40]. Considering the relatively large distance between ions (5.45 Å), the exchange interaction J_{nn} is expected to be weak and cannot be obtained with confidence from the susceptibility data.

In the susceptibility curve, there is no sharp magnetic ordering transition at any temperature $T \geq 2$ K. However, the change in gradient at $T < 10$ K (Fig. 6, inset) suggests the presence of a broad transition, e.g. due to short-range ordering. In the tripod kagome lattice family $A_2Tb_3Sb_3O_{14}$, the compounds with A = Mg and Zn both show a similar broad feature in the specific heat capacity C_{mag} around $1.5 - 2.5$ K, which the authors attribute to the nuclear spin degree of freedom of the Tb^{3+} ion (^{159}Tb, $I = 3/2$), although no such peak is visible in the susceptibility curves [41]. The susceptibility feature in our measurements may alternatively arise from one of the two crystallographically unique Tb^{3+} ions forming a singlet state. Such behaviour was observed in $TbInO_3$, which has a similar triangular lattice of inequivalent Tb^{3+} ions; however, one-third of the ions in $TbInO_3$ have a singlet ground state with a gap of $\Delta = 7.5$ K to the first excited state, while the remaining two-thirds have a doublet ground state, producing an effective honeycomb lattice at $T < \Delta$ [22]. The zero-field heat capacity of $Ba_3Tb(BO_3)_3$ (Fig. 7) shows a broad peak in C_{mag}/T at $T \approx 6$ K which is consistent with the hypothesis of short-range ordering in this temperature range. The magnetic entropy was estimated by integration of C/T as 4.2 J mol^{-1} K^{-1}, which is just under 20 % of the maximum magnetic entropy $R\ln(2J+1) = 21.32$ J mol^{-1} K^{-1}. Neutron scattering and/or further magnetometry and heat capacity measurements on $Ba_3Tb(BO_3)_3$ below 2 K are required in order to elucidate the exact reason for the observed behaviour.

Isothermal magnetisation was measured as a function of applied field using a Quantum Design PPMS (Fig. 8). At low temperatures, $T \leq 20$ K, there is some curvature but no sign of saturation in fields up to 14 T. The magnetisation at 2 K and 14 T, 5.27 μ_B per formula unit (f.u.), is significantly lower than that expected for a fully spin-polarised sample, $g_J J = 9$ μ_B/f.u., indicating strong single-ion anisotropy. The data for this new phase of $Ba_3Tb(BO_3)_3$ strongly resemble recent measurements on $KBaTb(BO_3)_2$
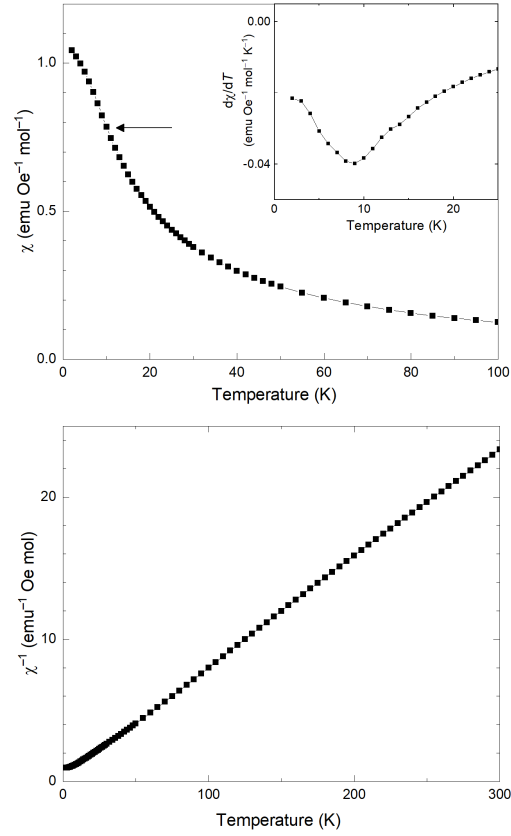
Figure 6: Top: Magnetic susceptibility as a function of temperature for the new hexagonal phase of $Ba_3Tb(BO_3)_3$ (inset: $d\chi/dT$ at low temperatures). The arrow indicates the location of the minimum in $d\chi/dT$ at $T = 9$ K. Bottom: Reciprocal magnetic susceptibility, χ^{-1}.
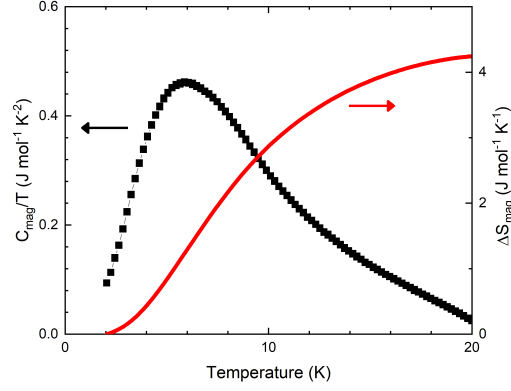
Figure 7: Magnetic heat capacity C_{mag}/T and entropy ΔS of $Ba_3Tb(BO_3)_3$ ($P6_3cm$) in the range 2–20 K.

Table 2: Bulk magnetic properties of $Ba_3Tb(BO_3)_3$ ($P6_3cm$): f.u. = formula unit.

	Low-T fit	High-T fit
T_0 (K)	< 2	< 2
θ_{CW} (K)	−7.15(14)	−9.8(2)
f	> 3.5	> 4.9
Experimental μ_{eff} (μ_B)	10.6(2)	10.3(2)
Theoretical μ_{eff} (μ_B)	9.72	9.72
$g_J J$	9	9
$M_{2K,14T}$ (μ_B/f.u.)	5.27(11)	5.27(11)

13

and RbBaTb$(BO_3)_2$, which also contain triangular lattices of Tb^{3+} ions, and where the magnetisation also reaches approximately 4.5 μ_B/f.u. at 2 K, 9 T [14, 15]. Magnetic measurements on a single crystal at different orientations to the applied field, along with CEF calculations from inelastic neutron scattering, would be required to confirm the local single-ion anisotropy of $Ba_3Tb(BO_3)_3$.
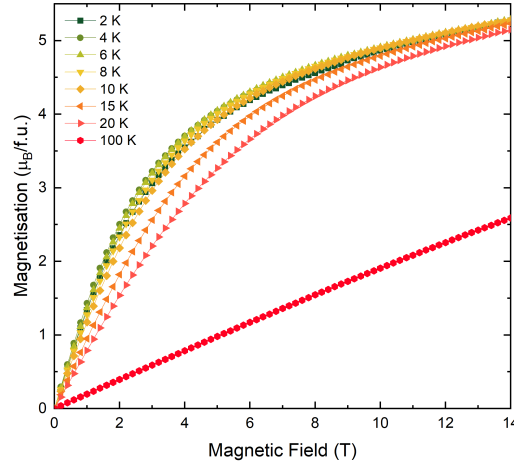

Figure 8: Isothermal magnetisation curves for the new hexagonal phase of $Ba_3Tb(BO_3)_3$.

3.3. Magnetocaloric effect

The lowering of the magnetic ordering temperature due to frustration is exploited in magnetic refrigeration applications in order to reduce usage of liquid helium [42]. Such devices make use of the magnetocaloric effect (MCE) to lower the sample temperature by adiabatic demagnetisation. The strongest MCE is observed in compounds containing Gd^{3+} due to its large effective magnetic moment (7.98 μ_B) and weak crystal field interactions; the best known ceramic material is gadolinium gallium garnet (GGG) which consists of interlinked corner-sharing triangles of spins [43, 44]. In general the MCE is maximised in high fields ($\mu_0 H > 5$ T), where Heisenberg systems have been shown to produce the greatest MCE. At low fields $\mu_0 H \leq 2$ T, systems with significant single-ion anisotropy (usually containing lanthanides other than Gd) tend to perform better [45].

In order to calculate the MCE, isothermal magnetisation measurements were made at temperatures $T = 2, 4, 6, 8$ and 10 K at field intervals of $\mu_0 H = 0.2$ T. The magnitude of the MCE for $Ba_3Tb(BO_3)_3$ was quantified by calculating the change in magnetic entropy per mole, ΔS_m, according to the Maxwell thermodynamic relation [42]:

$$\Delta S_m = \int_{H_0}^{H_1} \left(\frac{\partial M}{\partial T} \right)_H dH \tag{1}$$

before converting ΔS into gravimetric units (J K^{-1} kg^{-1}). While the molar MCE can be compared with the theoretical maximum ΔS_m for each lanthanide ion – dependent on the electronic configuration – the gravimetric MCE is more useful in comparing materials for practical application in devices.

The MCE is generally much weaker for Tb-containing compounds than their Gd analogues at equivalent fields and temperatures, due to the strong single-ion anisotropy of Tb^{3+} compared with Gd^{3+} [45–47]. However, at low fields and moderate temperatures (4–10 K) some Tb-containing compounds have shown better magnetocaloric performance than their Gd analogues. Due in part to the large relative atomic mass of Ba, the maximum MCE of $Ba_3Tb(BO_3)_3$ is very low compared with these benchmarks: in a field of 5 T, $Ba_3Tb(BO_3)_3$ has $-\Delta S_{max} = 1.22$ J K^{-1} kg^{-1}, while $Tb(HCO_2)_3$ and $TbOHCO_3$ have 15.7 and 33.72 J K^{-1} kg^{-1} respectively [45, 48].

The magnetocaloric data are plotted as a function of field and temperature in Fig. 9 using the convention of plotting $-\Delta S$, where a larger number indicates a stronger MCE. Data at intermediate temperature and field values were linearly interpolated.

The MCE shows features that are not expected for a material in a purely paramagnetic regime. At all fields $0 \leq \mu_0 H(T) \leq 14$ a maximum in $-\Delta S$ is observed at $T \approx 8 - 9$ K, and on further cooling ΔS becomes positive. The maximum in $-\Delta S$ is at a similar temperature to the minimum in $d\chi/dT$ observed in the susceptibility measurement and may therefore indicate magnetic ordering, as observed in the substituted gallium garnets $Ln_3MnGa_4O_{12}$ (Ln = Tb, Dy, Ho) [49]. Inverse MCE ($\Delta S > 0$) is uncommon but has been observed due to crystal electric field effects in $PrNi_5$ [42, 50], in transition metal alloys with first-order magnetic transitions [51], and in uniaxial paramagnets containing non-Kramers ions (Pr, Tb, Ho, and Tm) [52]. Susceptibility and
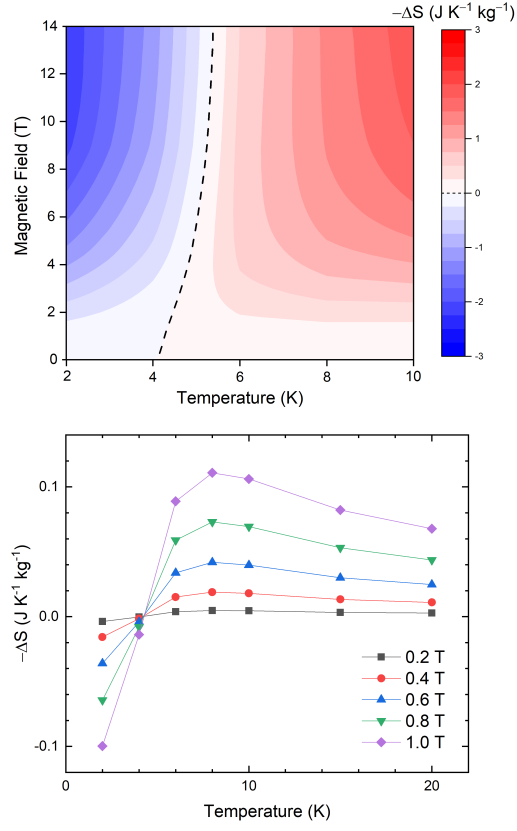
Figure 9: Magnetocaloric data for the new hexagonal phase of $Ba_3Tb(BO_3)_3$. Top: $-\Delta S(H, T)$; the dashed line indicates $\Delta S = 0$ (interpolated). Bottom: $-\Delta S(T)$ at fields $\mu_0 H \leq 1$ T.

specific heat measurements at fields ≥ 500 Oe and further $M(H)$ curves at smaller temperature intervals are planned in order to investigate this behaviour in $Ba_3Tb(BO_3)_3$.

4. Conclusions

We have synthesised a new hexagonal polymorph of $Ba_3Tb(BO_3)_3$ and measured its bulk magnetic properties. The new phase is isostructural with the heavier analogues $Ba_3Ln(BO_3)_3$ (Ln = Dy–Lu) where the arrangement of the Ln^{3+} ions forms a quasi-2D triangular lattice. PXRD measurements confirm that there is no magnetic site disorder and that the layers of Tb^{3+} ions are well separated. Magnetic measurements indicate that, like its heavier analogues, the title compound has antiferromagnetic interactions with no 3D magnetic ordering transition above 2 K, although there is evidence for possible short-range magnetic ordering and/or field-induced ordering in the $\chi'(T)$ and $M(H)$ data. Further experiments including measurements at $T < 2$ K are required in order to determine the nature of this ordering and to investigate the magnetic ground state. In contrast to e.g. $YbMgGaO_4$, the Ln^{3+} ions in $Ba_3Ln(BO_3)_3$ have well-defined environments as there is no non-magnetic site disorder.

Future work will investigate the possibility of forming an isostructural polymorph of $Ba_3Gd(BO_3)_3$, which may be of interest for magnetic refrigeration at liquid helium temperatures due to the large MCE associated with Gd^{3+} ions. Further work will focus on the synthesis of $Ba_3Ln(BO_3)_3$ (Ln = Tb–Yb) at different temperatures in an attempt to resolve disputes in the literature regarding the high-T phase behaviour.

5. Acknowledgments

6. Additional information

The authors declare that there are no competing interests.

Supplementary information is available: doi.org/xxxxxxxxx

Data relating to this publication are available: doi.org/yyyyyyyyy

The structure reported in this manuscript has been deposited with the Cambridge Crystallographic Data Centre: CSD 2010478.

References

[1] A. P. Ramirez, Strongly geometrically frustrated magnets, Annu. Rev. Mater. Sci. 24 (1) (1994) 453–480.

[2] M. F. Collins, O. A. Petrenko, Triangular antiferromagnets with a layered structure in a uniform field, Can. J. Phys. 75 (1997) 605–655.

[3] A. Banerjee, C. A. Bridges, J. Q. Yan, A. A. Aczel, L. Li, M. B. Stone, G. E. Granroth, M. D. Lumsden, Y. Yiu, J. Knolle, S. Bhattacharjee, D. L. Kovrizhin, R. Moessner, D. A. Tennant, D. G. Mandrus, S. E. Nagler, Proximate Kitaev quantum spin liquid behaviour in a honeycomb magnet, Nat. Mater. 15 (7) (2016) 733–740. doi:10.1038/nmat4604.

[4] J. Knolle, R. Moessner, A Field Guide to Spin Liquids, Annu. Rev. Condens. Matter Phys. 10 (1) (2019) 451–472.

[5] Y. Li, H. Liao, Z. Zhang, S. Li, F. Jin, L. Ling, L. Zhang, Y. Zou, L. Pi, Z. Yang, J. Wang, Z. Wu, Q. Zhang, Gapless quantum spin liquid ground state in the two-dimensional spin-1/2 triangular antiferromagnet YbMgGaO$_4$, Sci. Rep. 5 (October) (2015) 16419. doi:10.1038/srep16419.

[6] J. G. Rau, M. J. Gingras, Frustration and anisotropic exchange in ytterbium magnets with edge-shared octahedra, Phys. Rev. B 98 (2018) 054408. doi:10.1103/PhysRevB.98.054408.

[7] Y. Li, P. Gegenwart, A. A. Tsirlin, Spin liquids in geometrically perfect triangular antiferromagnets, J. Phys. Condens. Matter 32 (2020) 224004. doi:10.1088/1361-648X/ab724e.

[8] J. A. M. Paddison, M. Daum, Z. Dun, G. Ehlers, Y. Liu, M. B. Stone, H. Zhou, M. Mourigal, Continuous excitations of the triangular-lattice quantum spin liquid YbMgGaO$_4$, Nat. Phys. 13 (2) (2017) 117–122. doi:10.1038/nphys3971.

[9] Y. Li, D. T. Adroja, R. I. Bewley, D. Voneshen, A. A. Tsirlin, P. Gegenwart, Q. Zhang, Crystalline Electric-Field Randomness in the Triangular Lattice Spin-Liquid YbMgGaO$_4$, Phys. Rev. Lett. 118 (2017) 107202. doi:10.1103/PhysRevLett.118.107202.

[10] Z. Zhu, P. A. Maksimov, S. R. White, A. L. Chernyshev, Disorder-Induced Mimicry of a Spin Liquid in YbMgGaO$_4$, Phys. Rev. Lett. 119 (2017) 157201. doi:10.1103/PhysRevLett.119.157201.

[11] Z. Ma, J. Wang, Z. Y. Dong, J. Zhang, S. Li, S. H. Zheng, Y. Yu, W. Wang, L. Che, K. Ran, S. Bao, Z. Cai, P. Čermák, A. Schneidewind, S. Yano, J. S. Gardner, X. Lu, S. L. Yu, J. M. Liu, S. Li, J. X. Li, J. Wen, Spin-Glass Ground State in a Triangular-Lattice Compound YbZnGaO$_4$, Phys. Rev. Lett. 120 (2018) 087201. doi:10.1103/PhysRevLett.120.087201.

[12] M. Ashtar, Y. X. Gao, C. L. Wang, Y. Qiu, W. Tong, Y. M. Zou, X. W. Zhang, M. A. Marwat, S. L. Yuan, Z. M. Tian, Synthesis, structure and magnetic properties of rare-earth REMgAl$_{11}$O$_{19}$ (RE = Pr, Nd) compounds with two-dimensional triangular lattice, J. Alloys Compd. 802 (2019) 146–151. doi:10.1016/j.jallcom.2019.06.177.

[13] J. Gao, L. Song, X. Hu, D. Zhang, A buetschliite-type rare-earth borate, KBaY(BO$_3$)$_2$, Solid State Sci. 13 (1) (2011) 115–119. doi:10.1016/j.solidstatesciences.2010.10.021.

[14] M. B. Sanders, F. A. Cevallos, R. J. Cava, Magnetism in the KBaRE(BO$_3$)$_2$ (RE = Sm, Eu, Gd, Tb, Dy, Ho, Er, Tm, Yb, Lu) series: Materials with a triangular rare earth lattice, Mater. Res. Express 4 (3) (2017) 036102. doi:10.1088/2053-1591/aa60a2.

[15] S. Guo, T. Kong, W. Xie, L. Nguyen, K. Stolze, F. A. Cevallos, R. J. Cava, Triangular Rare-Earth Lattice Materials RbBaR(BO$_3$)$_2$ (R = Y, Gd–Yb) and Comparison to the KBaR(BO$_3$)$_2$ Analogs, Inorg. Chem. 58 (5) (2019) 3308–3315. doi:10.1021/acs.inorgchem.8b03372.

[16] L. Ding, P. Manuel, S. Bachus, F. Grußler, P. Gegenwart, J. Singleton, R. D. Johnson, H. C. Walker, D. T. Adroja, A. D. Hillier, A. A. Tsirlin, Gapless spin-liquid state in the structurally disorder-free triangular antiferromagnet NaYbO$_2$, Phys. Rev. B 100 (2019) 144432. doi:10.1103/PhysRevB.100.144432.

[17] M. M. Bordelon, E. Kenney, C. Liu, T. Hogan, L. Posthuma, M. Kavand, Y. Lyu, M. Sherwin, N. P. Butch, C. Brown, M. J. Graf, L. Balents, S. D. Wilson, Field-tunable quantum disordered ground state in the triangular-lattice antiferromagnet NaYbO$_2$, Nat. Phys. 15 (2019) 1058–1064. arXiv:1901.09408, doi:10.1038/s41567-019-0594-5.

[18] A. I. Smirnov, L. E. Svistov, L. A. Prozorova, A. Zheludev, M. D. Lumsden, E. Ressouche, O. A. Petrenko, K. Nishikawa, S. Kimura, M. Hagiwara, K. Kindo, A. Y. Shapiro, L. N. Demianets, Chiral and collinear ordering in a distorted triangular antiferromagnet, Phys. Rev. Lett. 102 (2009) 037202. doi:10.1103/PhysRevLett.102.037202.

[19] R. S. Fishman, S. Okamoto, Noncollinear magnetic phases of a triangular-lattice antiferromagnet and of doped CuFeO$_2$, Phys. Rev. B - Condens. Matter Mater. Phys. 81 (2010) 020402(R). doi:10.1103/PhysRevB.81.020402.

[20] S. E. Dutton, E. Climent-Pascual, P. W. Stephens, J. P. Hodges, A. Huq, C. L. Broholm, R. J. Cava, Helical magnetism and structural anomalies in triangular lattice α-SrCr$_2$O$_4$, J. Phys. Condens. Matter 23 (2011) 246005.

[21] L. C. Chapon, P. Manuel, F. Damay, P. Toledano, V. Hardy, C. Martin, Helical magnetic state in the distorted triangular lattice of α-CaCr$_2$O$_4$, Phys. Rev. B - Condens. Matter Mater. Phys. 83 (2011) 024409. doi:10.1103/PhysRevB.83.024409.

[22] L. Clark, G. Sala, D. D. Maharaj, M. B. Stone, K. S. Knight, M. T. Telling, X. Wang, X. Xu, J. Kim, Y. Li, S. W. Cheong, B. D. Gaulin, Two-dimensional spin liquid behaviour in the triangular-honeycomb antiferromagnet $TbInO_3$, Nat. Phys. 15 (3) (2019) 262–268. doi:10.1038/s41567-018-0407-2.

[23] A. Ilyukhin, B. Dzhurinskij, Crystal structures of binary borates LnBa$_3$(BO$_3$)$_3$ (Ln = Dy, Ho, Tm, Yb, and Lu), Russ. J. Inorg. Chem. 38 (1993) 1625–1630.

[24] K. I. Schaffers, P. D. Thompson, T. Alekel, J. R. Cox, D. A. Keszler, STACK Crystal Chemistry, Chem. Mater. 6 (11) (1994) 2014–2022. doi:10.1021/cm00047a022.
URL https://pubs.acs.org/doi/abs/10.1021/cm00047a022

[25] T. N. Khamaganova, N. M. Kuperman, Z. G. Bazarova, The Double Borates Ba$_3$$Ln$(BO$_3$)$_3$, Ln=La-Lu, Y, J. Solid State Chem. 145 (1) (1999) 33–36. doi:10.1006/jssc.1999.8163.

[26] Y. Gao, L. Xu, Z. Tian, S. Yuan, Synthesis and magnetism of RE(BaBO$_3$)$_3$ (RE=Dy,Ho,Er,Tm,Yb) series with rare earth ions on a two dimensional triangle-lattice, J. Alloys Compd. 745 (2018) 396–400. doi:10.1016/j.jallcom.2018.02.110.

[27] K. Y. Zeng, L. Ma, Y. X. Gao, Z. M. Tian, L. S. Ling, L. Pi, NMR evidence for gapless quantum spin liquid state in the ideal triangular-lattice compound Yb(BaBO$_3$)$_3$ (2019). arXiv:1912.03814.

[28] H. M. Rietveld, A profile refinement method for nuclear and magnetic structures, J. Appl. Crystallogr. 2 (2) (1969) 65–71. doi:10.1107/S0021889869006558.

[29] A. A. Coelho, TOPAS and TOPAS-Academic: An optimization program integrating computer algebra and crystallographic objects written in C++, J. Appl. Crystallogr. 51 (1) (2018) 210–218. doi:10.1107/S1600576718000183.

[30] D. Smith, F. Fickett, Low-Temperature Properties of Silver, J. Res. Natl. Inst. Stand. Technol. 100 (2) (1995) 119. doi:10.6028/jres.100.012.

[31] E. S. R. Gopal, Lattice Heat Capacity, in: E. S. R. Gopal (Ed.), Specif. Heats Low Temp., Springer US, Boston, MA, 1966, pp. 20–54.

[32] J. R. Cox, D. A. Keszler, J. Huang, The Layered Borates $Ba_3M(BO_3)_3$ (M = Dy, Ho, Y, Er, Tm, Yb, Lu, and Sc), Chem. Mater. 6 (11) (1994) 2008–2013. doi:10.1021/cm00047a021.

[33] R. D. Shannon, Revised Effective Ionic Radii and Systematic Studies of Interatomic Distances in Halides and Chalcogenides, Acta Crystallogr. A32 (1976) 751–767.

[34] P. Mukherjee, Y. Wu, G. I. Lampronti, S. E. Dutton, Magnetic properties of monoclinic lanthanide orthoborates, LnBO$_3$, Ln = Gd, Tb, Dy, Ho, Er, Yb, Mater. Res. Bull. 98 (2018) 173–179. doi:10.1016/j.materresbull.2017.10.007.

[35] R. Simura, S. Kawai, K. Sugiyama, Phase Transition and Thermal Expansion of Ba_3RB$_3$O$_9$ (R = Sm-Yb, and Y), High Temp. Mater. Process. 36 (8) (2017) 763–769. doi:10.1515/htmp-2015-0290.

[36] T. N. Khamaganova, N. M. Khrushcheva, N. E. Astakhov, Synthesis of rhombohedral borates $Ba_3R(BO_3)_3$, R = Pr-Dy, Russ. J. Appl. Chem. 82 (12) (2009) 2214–2216.

[37] W. T. Chen, C. Ablitt, N. C. Bristowe, A. A. Mostofi, T. Saito, Y. Shimakawa, M. S. Senn, Negative thermal expansion in high pressure layered perovskite Ca_2GeO_4, Chem. Commun. 55 (20) (2019) 2984–2987. doi:10.1039/c8cc09614g.

[38] C. R. Morelock, B. K. Greve, M. Cetinkol, K. W. Chapman, P. J. Chupas, A. P. Wilkinson, Role of anion site disorder in the near zero thermal expansion of tantalum oxyfluoride, Chem. Mater. 25 (9) (2013) 1900–1904. doi:10.1021/cm400536n.

[39] M. Baise, P. M. Maffettone, F. Trousselet, N. P. Funnell, F. X. Coudert, A. L. Goodwin, Negative Hydration Expansion in ZrW_2O_8: Microscopic Mechanism, Spaghetti Dynamics, and Negative Thermal Expansion, Phys. Rev. Lett. 120 (2018) 265501. doi:10.1103/PhysRevLett.120.265501.

[40] M. J. Gingras, B. C. den Hertog, M. Faucher, J. S. Gardner, S. R. Dunsiger, L. J. Chang, B. D. Gaulin, N. P. Raju, J. E. Greedan, Thermodynamic and single-ion properties of Tb^{3+} within the collective paramagnetic-spin liquid state of the frustrated pyrochlore antiferromagnet $Tb_2Ti_2O_7$, Phys. Rev. B - Condens. Matter Mater. Phys. 62 (2000) 6496–6511. doi:10.1103/PhysRevB.62.6496.

[41] Z. L. Dun, J. Trinh, M. Lee, E. S. Choi, K. Li, Y. F. Hu, Y. X. Wang, N. Blanc, A. P. Ramirez, H. D. Zhou, Structural and magnetic properties of two branches of the tripod-kagome-lattice family $A_2R_3Sb_3O_{14}$ (A = Mg, Zn; R = Pr, Nd, Gd, Tb, Dy, Ho, Er, Yb), Phys. Rev. B 95 (2017) 104439. doi:10.1103/PhysRevB.95.104439.

[42] V. K. Pecharsky, K. A. Gschneidner, Magnetocaloric effect and magnetic refrigeration, J. Magn. Magn. Mater. 200 (1-3) (1999) 44–56. doi:10.1016/S0304-8853(99)00397-2.

[43] J. A. Barclay, W. A. Steyert, Materials for magnetic refrigeration between 2 K and 20 K, Cryogenics (Guildf). 22 (1982) 73–80.

[44] R. Moessner, Magnets with strong geometric frustration, Can. J. Phys. 79 (11-12) (2001) 1283–1294. doi:10.1139/p01-123.

[45] P. J. Saines, J. A. M. Paddison, P. M. M. Thygesen, M. G. Tucker, Searching beyond Gd for magnetocaloric frameworks: magnetic properties and interactions of the $Ln(HCO_2)_3$ series, Mater. Horizons 2 (5) (2015) 528–535. doi:10.1039/c5mh00113g.

[46] T. Numazawa, K. Kamiya, T. Okano, K. Matsumoto, Magneto caloric effect in $(Dy_xGd_{1-x})_3Ga_5O_{12}$ for adiabatic demagnetization refrigeration, Phys. B Condens. Matter 329-333 (2003) 1656–1657. doi:10.1016/S0921-4526(02)02447-X.

[47] N. A. Spaldin, Magnetic Materials: Fundamentals and Applications, 2nd Edition, Cambridge University Press, Cambridge, 2011.

[48] R. J. Dixey, P. J. Saines, Optimization of the Magnetocaloric Effect in Low Applied Magnetic Fields in LnOHCO$_3$ Frameworks, Inorg. Chem. 57 (2018) 12543–12551. doi:10.1021/acs.inorgchem.8b01549.

[49] P. Mukherjee, Investigation of the magnetic and magnetocaloric properties of complex lanthanide oxides, Phd, University of Cambridge (2018). doi:10.17863/CAM.22636.

[50] P. von Ranke, V. K. Pecharsky, K. Gschneidner, Anomalous behavior of the magnetic entropy in PrNi$_5$, Phys. Rev. B 58 (1998) 14436–14441. doi:10.1103/PhysRevB.58.14436.

[51] T. Krenke, E. Duman, M. Acet, E. F. Wassermann, X. Moya, L. Manosa, A. Planes, Inverse magnetocaloric effect in ferromagnetic Ni-Mn-Sn alloys, Nat. Mater. 4 (2005) 450–454. doi:10.1038/nmat1395.

[52] E. E. Kokorina, M. V. Medvedev, Inverse magnetocaloric effect in the uniaxial paramagnet with non-Kramers ions, Phys. Met. Metallogr. 118 (2017) 217–226. doi:10.1134/S0031918X17010021.